# Another Look at Downslope Windstorms. Part I: The Development of Analogs to Supercritical Flow in an Infinitely Deep, Continuously Stratified Fluid

DALE R. DURRAN

*Department of Meteorology, University of Utah, Salt Lake City, UT 84112*

(Manuscript received 24 October 1985, in final form 12 May 1986)

ABSTRACT

Numerical simulations are conducted to examine the role played by different amplification mechanisms in the development of large-amplitude mountain waves. It is shown that when the static stability has a two-layer structure, the nonlinear response can differ significantly from the solution to the equivalent linear problem when the parameter $Nh/U$ is as small as 0.3. In the cases where the nonlinear waves are much larger than their linear counterparts, the highest stability is found in the lower layer and the flow resembles a hydraulic jump. Simulations of the 11 January 1972 Boulder windstorm are presented which suggest that the transition to supercritical flow, forced by the presence of a low-level inversion, plays an essential role in triggering the windstorm. The similarities between breaking waves and nonbreaking waves which undergo a transition to supercritical flow are discussed.

## 1. Introduction

Every few years the eastern slope of the Colorado Front Range (part of the Rocky Mountains) experiences a damaging downslope windstorm, with peak gusts as high as 60 m $s^{-1}$. Similar winds are also observed along the lee slopes of many other mountain barriers. The local names for these winds include the Alpine Foehn, the Rocky Mountain Chinook, the Yugoslavian Bora, and the Argentine Zonda. Although downslope winds have been studied extensively for more than 30 years, their dynamics are still not satisfactorily understood. At present, there are three different mechanisms that have been proposed to account for the development of strong downslope winds.

One mechanism is based on hydraulic theory (Long, 1954; Houghton and Kasahara, 1968), in which the airflow over a mountain is modeled by fluid flowing over an obstacle. According to hydraulic theory, strong winds will occur along the lee slope when the fluid undergoes a transition from subcritical flow upstream to supercritical flow over the mountain. This approach has the advantage of explicitly accounting for the nonlinearity introduced by mountains of finite height. However, it also suffers from the disadvantage that the top of the fluid must be bounded by a rigid lid or a free surface, both of which prevent the vertical propagation of energy possible in the real atmosphere.

A second mechanism is based on the linear theory of internal gravity waves in a continuously stratified, semi-infinite fluid. Any vertically propagating gravity wave which transports energy upwards produces a disturbance which is asymmetric about the mountain peak, with strong winds and low pressure over the lee slope. When an upward propagating wave encounters a region in which the Scorer parameter changes rapidly, part of its energy is reflected back into a downward propagating mode. The wave amplitude below the reflecting layer is thus determined by the superposition of upward and downward propagating waves. Klemp and Lilly (1975) suggested that strong downslope winds occur when the atmosphere has a multilayer structure which produces an optimal superposition of these upward and downward propagating components. Their approach has the advantage that it can accommodate very realistic wind and stability profiles. However, since it relies on linear theory, the applicability of their work to large-amplitude waves has yet to be firmly established.

The third mechanism is based on results obtained from numerical integrations of the equations which govern the dynamics of the flow. In a series of papers, Clark and Peltier (1977, 1984), and Peltier and Clark, (1979, 1983), and Clark and Farley (1984) have suggested that large-amplitude waves and downslope winds are produced after a developing wave breaks. The wave-breaking region is characterized by strong mixing and a local reversal of the cross-mountain wind. Clark and Peltier suggest that the energy in the upward propagating wave is trapped below this "self-induced critical layer," producing a substantial increase in the wave amplitude. Their numerical approach has the advantage that it both explicitly accounts for finite amplitude effects and allows a detailed representation of the atmospheric flow structure. However, numerical results are often more difficult to interpret than those which have been obtained analytically. At present there is still some controversy about the influence of self-in-

duced critical layers on the subsequent amplification of the wave (Lilly and Klemp, 1980; Peltier and Clark 1980). Smith (1985) has recently obtained analytic solutions to Long's equation for the flow beneath a breaking wave, by assuming that the air in the overturned region has been mixed so that it is neutrally stratified. His solutions do not include any explicit representation of a critical layer.

The linear theory of vertically propagating waves predicts that some enhancement of the leeside winds will be produced by arbitrarily small mountains, whereas hydraulic theory (at least to the accuracy of the shallow water approximation) suggests that downslope winds will only occur if the mountain height exceeds the threshold required to force a transition to supercritical flow. Thus, one fundamental difference between the amplification mechanisms described by Long (1954), and by Lilly and Klemp (1975), is that the former relies on nonlinear phenomena, while the latter depends only on linear processes. The theories of Clark and Peltier, and Smith might be considered theories for the development of very nonlinear waves inasmuch as the wave breaking mechanism will not become active (at least in the upper troposphere) unless a rather large amplitude wave has already been produced by other physical processes. The purpose of this paper is to examine the role played by hydraulics and vertically propagating internal waves on the development of large-amplitude waves. The remainder of the paper is organized as follows. The numerical model, which serves as a basic tool in this study, is described in section 2. The effect of finite amplitude on vertically propagating waves in multilayer atmospheres is examined in section 3. The results obtained in section 3 are put more clearly into focus in the discussion in section 4. The relative importance of each amplification mechanism on the development of wave breaking and downslope winds in simulations of the 11 January 1972 Boulder windstorm is described in section 5. Wave breaking in an atmosphere with constant mean windspeed and stability is examined in section 6. Section 7 contains the conclusion.

## 2. The numerical model

The computer simulations presented in this paper were obtained using a numerical model designed to calculate the two-dimensional airflow over an infinitely long, uniform mountain barrier. The Coriolis force is neglected, since we will consider only high Rossby number flow. The effect of moisture is also neglected. Under these assumptions, the equations which govern the waves may be written:

$$\frac{du}{dt}+c_p\theta\frac{\partial\pi}{\partial x}=D_u, \tag{1}$$

$$\frac{dw}{dt}+c_p\theta\frac{\partial\pi}{\partial z}=g\frac{(\theta-\bar{\theta})}{\bar{\theta}}+D_w, \tag{2}$$

$$\frac{d\pi}{dt}+w\frac{d\bar{\Pi}}{dz}+\frac{R}{c_v}(\bar{\Pi}+\pi)\left(\frac{\partial u}{\partial x}+\frac{\partial w}{\partial z}\right)-\frac{R}{c_v}\frac{(\bar{\Pi}+\pi)}{\theta}\frac{d\theta}{dt}=0, \tag{3}$$

$$\frac{d\theta}{dt}=D_\theta, \tag{4}$$

where

$$\left.\begin{aligned}\frac{d}{dt}&=\frac{\partial}{\partial t}+u\frac{\partial}{\partial x}+w\frac{\partial}{\partial z},\\ \bar{\Pi}+\pi&=\left(\frac{p}{p_0}\right)^{R/c_p}\end{aligned}\right\} \tag{5}$$

In the above, $p$ is the pressure, $p_0$ = 1000 mb, $R$ is the gas constant for dry air, $c_p$ is the specific heat of dry air at constant pressure, $c_v$ the specific heat at constant volume, $\theta$ the potential temperature, and $u$ and $w$ are the horizontal and vertical velocity components. Overbars denote the undisturbed, horizontally homogeneous mean state. The $D$ terms contain the contributions from subgrid scale mixing, which is parameterized as a function of the larger scale flow via a first-order closure formulation which depends on the relative strengths of the stratification and shear; the mathematical formulae for $D_u$, $D_w$ and $D_\theta$ are given in the Appendix. A free-slip boundary condition is imposed at the surface; the surface topography is included by a coordinate transformation.

The numerical model solves these equations in a computationally efficient manner by treating the sound wave modes separately on a shorter time step. The bulk of the computation is done on the large time step. In the large time step, the time differencing is leapfrog, horizontal advection is fourth order, and vertical advection is second order. Buoyancy, diffusion and coordinate transformation terms are computed to at least second-order accuracy. Wave permeable lateral and upper boundaries are specified according to the numerical prescriptions of Orlanski (1976) and Klemp and Durran (1983). A complete description of the numerical model and a thorough discussion of its testing and verification can be found in Durran and Klemp (1983).

## 3. The effects of finite amplitude on vertically propagating waves in multilayer atmospheres

In the following, we will investigate the extent to which linear mountain wave theory can be applied to situations for which the linearization assumptions are not formally valid. A satisfactory treatment of this question has already been given for the special case in which the undisturbed profiles of $\rho U^2$ and $d\rho/dz$ are constant with height (within the accuracy of the Boussinesq approximation, an equivalent condition is that the mean windspeed $U$ and Brunt-Väisälä frequency

$N$ are constant with height), in which case the steady state flow is governed by Long's equation (Long, 1953). Lilly and Klemp (1979) have shown that although nonlinear hydrostatic waves in an atmosphere with uniform stability and windspeed are somewhat stronger than their linear counterparts, the two solutions are qualitatively similar for all amplitudes less than that required to produce overturning. However, as noted by Smith (1977), the assumption of constant $N$ and $U$ places a special constraint on the nonlinear interactions possible in the steady flow.

In order to examine the effects of nonlinearity on vertically propagating waves when the mean state is more complex, we will rely on the numerical model. Consider a situation in which the windspeed is 20 m $s^{-1}$ and constant with height, and the Brunt-Väisälä frequency has a two-layer structure with $N = 0.01$ $s^{-1}$ or 0.02 $s^{-1}$ in each layer. The mountain profile is a "witch of Agnesi,"

$$z_s(x) = \frac{ha^2}{x^2 + a^2}, \tag{6}$$

where $a$ is the mountain half-width and $h$ the mountain height. In these simulations $a = 10$ km and $h = 1$ or 600 m. The numerical domain contains 120 points in the horizontal and 40 points in the vertical, $\Delta x = 1.5$ km, $\Delta z = 200$ m, and the large and small time steps are 10 s and 3.3 s respectively. The airflow is initialized by increasing the windspeed and gravity from zero to their actual values over a nondimensional time ($Ut/a$) of 4.

According to linear theory, there are four basic tuned or detuned cases which can occur when hydrostatic waves are present in a two-layer atmosphere. If the layer with the higher stability is on the bottom, the atmosphere will be tuned for the strongest response when there is a quarter-wavelength phase shift between the ground and the layer interface. It will be detuned, producing the weakest response, when the phase shift is one-half wavelength. The tuning characteristics are exactly reversed if the layer with the lower stability is on the bottom (i.e., strongest response when the phase shift is one-half wavelength). The four cases to be examined are summarized in Table 1.

A normalized pressure drag will be used as a measure of the strength of the wave response. It is calculated as the actual drag, divided by the drag associated with the linear waves which would be forced by an identical mountain if the windspeed and stability were constant with height and equal to the values found at the surface in the multilayer atmosphere. If it is assumed that the waves are steady, linear and hydrostatic, the normalized drag for cases 1–4 may be calculated analytically; these values are also given in Table 1.

The last two columns in Table 1 show the normalized drag, calculated with the numerical model, for pairs of simulations in which the mountain height was either 1 or 600 m. The results obtained using a 1 m high mountain are essentially linear solutions since the contributions from the nonlinear terms in the model are negligible. As may be observed in Table 1, the normalized drags obtained with the "linear" numerical model agree reasonably well with the analytic values. The differences are primarily due to nonsteadiness (the results given are for a dimensionless time, $Ut/a$, of 40 but cases 1 and 4 still exhibit a very slow drift toward higher values), nonhydrostatic effects (quantified at 5%–10% by running a hydrostatic version of the model), and discretization errors in representing the interface on the numerical mesh. It should also be noted that the drag, being a second-order quantity, is more sensitive to error than the velocity fields themselves.

The simulations with the 600 m mountain might be considered moderately nonlinear, in that the perturbations are large compared to the mean state but never exceed them. It should be emphasized that none of these waves reach sufficient amplitude to break or to activate the subgrid-scale turbulent mixing. The inverse Froude number, $Nh/U$, is a measure of nonlinearity which, in the cases under consideration, has a maximum value of 0.6. Lilly and Klemp (1979) have shown that if $Nh/U = 0.6$ and the windspeed and stability are constant with height, the normalized drag for a witch of Agnesi mountain is approximately 1.1. Inspection of Table 1 shows that the difference between the linear and nonlinear solutions can be far larger when a single-layer atmosphere is replaced with a two-layer structure. Note, in particular, the variety of the different responses. In cases 1 and 4, the amplification of the linear solution produced by the layered structure disappears when the flow is nonlinear. In case 2, the damping associated with the linear wave gives way to very strong amplification in the nonlinear regime. On the other

TABLE 1. Normalized pressure drag in a two-layer atmosphere.

| Case | $N_L$ ($s^{-1}$) | $N_U$ ($s^{-1}$) | $H$ (m) | Drag: Linear, analytic, hydrostatic | Drag: Linear, model, nonhydrostatic | Drag: Nonlinear, model, nonhydrostatic |
|---|---|---|---|---|---|---|
| 1 | 0.02 | 0.01 | 1571 | 2.0 | 1.5 | 1.0 |
| 2 | 0.02 | 0.01 | 3142 | 0.5 | 0.50 | 2.9 |
| 3 | 0.01 | 0.02 | 3142 | 0.5 | 0.53 | 0.53 |
| 4 | 0.01 | 0.02 | 6243 | 2.0 | 1.7 | 0.79 |

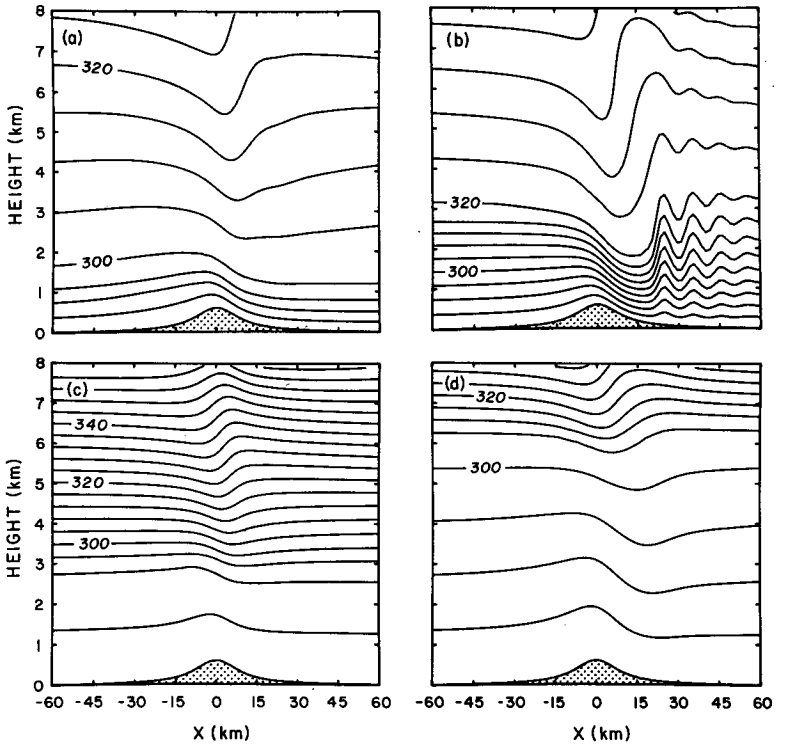


FIG. 1. Isentropes for the air in a two-layer atmosphere flowing over a 600 m high mountain at a nondimensional time $Ut/a = 20$. (a) case 1: interface at 1571 m, one-quarter wavelength; (b) case 2: interface at 3142 m, one-half wavelength; (c) case 3: interface at 3142 m, one-quarter wavelength; (d) case 4: interface at 6243 m, one-half wavelength. In this and all the figures which follow, the airflow is from left to right.

hand, the damping of the waves in case 3 seems to be unaffected by the increase in nonlinearity.

An examination of Fig. 1, which shows the isentropes for the airflow in each of the nonlinear solutions to cases 1–4, suggests that the character of the flow in case 2 may be considerably different from that in the other cases. In the other cases, the solution is dominated by a single vertically propagating wave (and is qualitatively similar to the linear solution). However, in case 2, the flow looks rather like a hydraulic jump. The trapped or partially trapped lee waves which appear in Fig. 1b, and many of the later figures, are eliminated by the hydrostatic approximation. The simulation of several cases with a hydrostatic version of the model has demonstrated that the lee waves play no fundamental role in the development of strong downslope winds and high pressure drag, suggesting, as was first hypothesized by Smith (1976), that "the hydrostatic part of the flow can be thought of as the forcing mechanism for the lee waves." This is demonstrated in Fig. 2, which shows the hydrostatic equivalent to Fig. 1b.

Since the downslope winds in case 2 far exceed the winds in the other cases we will examine this situation in more detail. Additional jumplike behavior is exhibited in the following experiments in which the height of the mountain and the height of the interface are varied in a two-layer atmosphere where $N$ is 0.01 and 0.025 $s^{-1}$ in the upper and lower layers, respectively, and the windspeed is a constant 25 m $s^{-1}$. The mountain half-width is 10 km, $\Delta x$ and $\Delta z$ are 1 km and 200 m, respectively, the numerical grid contains 150 points in the horizontal and 40 vertical levels. The mountain is centered at grid point 60.5; only the central portion of the domain is shown in these figures.

Figure 3 shows the isentropes for the flows which develop when the depth of the lowest layer is fixed at 3 km, and the height of the mountain is varied between 200 and 800 m. As the height of the mountain increases, a "shooting" flow appears along the lee slope. Trapped waves, which are not efficiently forced in the linear solution because the mountain is too wide, are excited to large amplitudes by the short wavelength forcing associated with the recovery of the shooting flow to the ambient downstream conditions. When the amplitude of the trapped waves becomes sufficiently large, they are destroyed by mixing. (However, the subgrid scale mixing was active only when the mountain height exceeded 500 m.) The region of strongest surface wind migrates down the lee slope as the flow develops a more jumplike character. As noted by Blu-

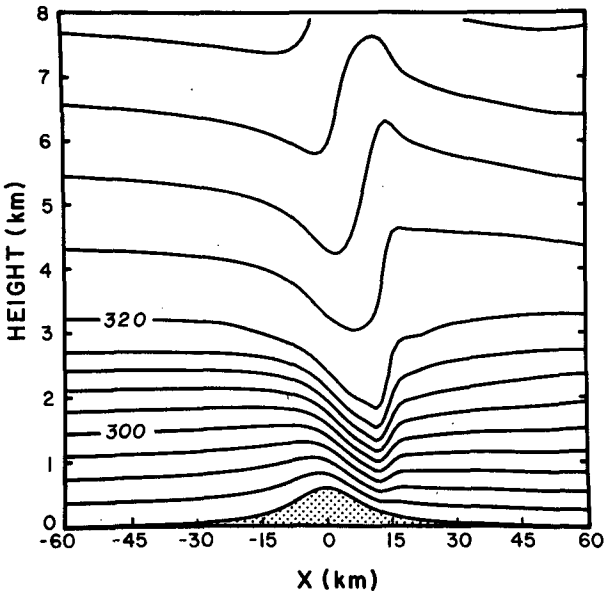


FIG. 2. As in Fig. 1b, except that the flow is constrained to be in hydrostatic balance.

men and Hartsough (1985), linear theory predicts that the speed maximum will occur between the center of the lee slope and the mountain crest; however, the strongest winds are often observed near the base of a mountain. These simulations suggest that finite amplitude effects are responsible for bringing high winds to the bottom of the mountain.

The normalized pressure drag across the mountain is plotted as a function of the mountain height in Fig. 4. One can clearly observe a dramatic increase in the drag as the mountain height increases from 200 to 500 m. A similar increase in the drag occurs in hydraulic theory as the height of the obstacle becomes sufficient to force a transition from subcritical flow upstream to supercritical flow at the crest.

Figure 5 shows the solutions obtained if the mountain height is fixed at 500 m and the depth of the lower layer is varied. It may be observed that the behavior of the interface is analogous to the behavior of the free surface of a homogenous fluid flowing over a barrier (Houghton and Kasahara, 1968; also see Fig. 9). As the depth of the lower layer increases, the interface first assumes a form similar to an everywhere-supercritical flow (Fig. 5a), then appears like a propagating hydraulic jump (Fig. 5b), a stationary jump (Fig. 5c), and finally like an everywhere-subcritical flow (Fig. 5d). The horizontal velocity fields associated with each of the runs in Fig. 5 are shown in Fig. 6. According to shallow water theory, if no hydraulic jumps are present, the velocity perturbations should be symmetric with respect to the mountain crest, with a decrease in speed

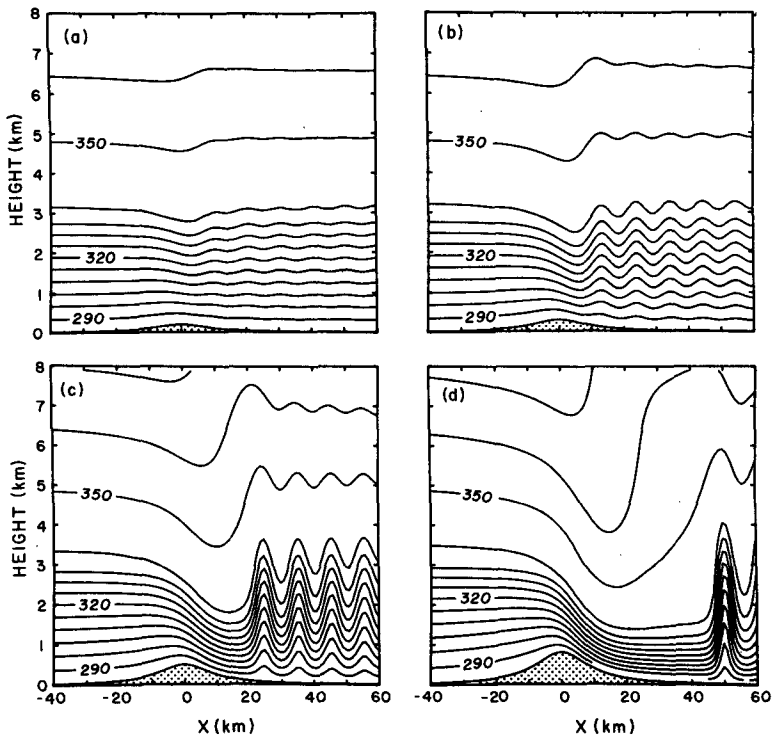


FIG. 3. Isentropes for the airflow in a two-layer atmosphere, at $Ut/a = 25$, when the interface is fixed at 3000 m, and the mountain height is (a) 200, (b) 300, (c) 500 and (d) 800 m.

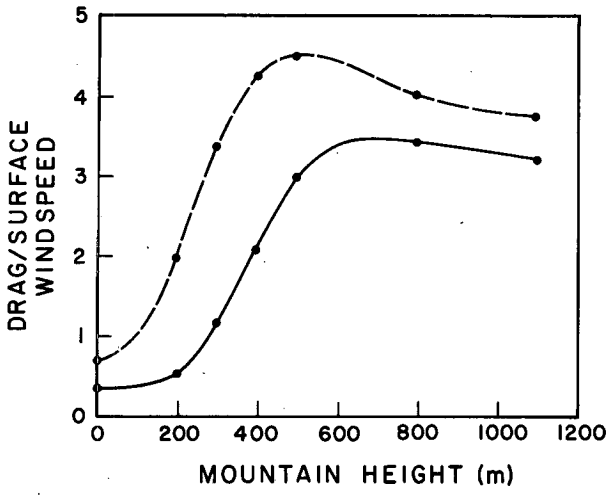


FIG. 4. Pressure drag (solid) and maximum surface windspeed perturbation (dashed) as a function of mountain height for a two-layer atmosphere with the interface at 3000 m. The drag is normalized by $\pi\rho NUh^2/4$ and the windspeed by $Nh/2$, where $\rho$, $U$ and $N$ are evaluated at the surface.

over the mountain in the everywhere-supercritical case, and an increase in speed in the everywhere-subcritical case. This qualitative behavior may be observed in Fig. 6a, d; however, it should be noted that the velocity field in each of these nonjumplike cases also bears a strong resemblance to that calculated from the solution for linear internal waves in the same two-layer atmosphere.

It might seem surprising that hydraulic-like behavior is encountered in the preceding simulations. Aside from the usual concerns about vertical energy propagation (allowed by the atmosphere but not accounted for in hydraulic theory), there is nothing, such as an elevated inversion in the upstream flow, which even approximates the discontinuity in density found at the free surface of a liquid. One approach that might be used to connect hydraulic theory with our results would be to define a Froude number as the ratio of the speed of the mean flow to the horizontal phase speed of some linear wave supported by the system. In an infinitely deep atmosphere there are always long wavelength, vertically propagating modes whose phase speed exceeds the mean flow, and the flow can never be supercritical (at least with respect to those modes). However, a two-layer atmosphere will also support $n$ trapped resonant waves whose phase speeds are

$$c=\frac{2H}{(2n-1)\pi}(N_L^2-N_U^2)^{1/2} \tag{7}$$

where $N_L$ and $N_U$ are the Brunt–Väisälä frequencies in the upper and lower layers; $H$ is the depth of the lower

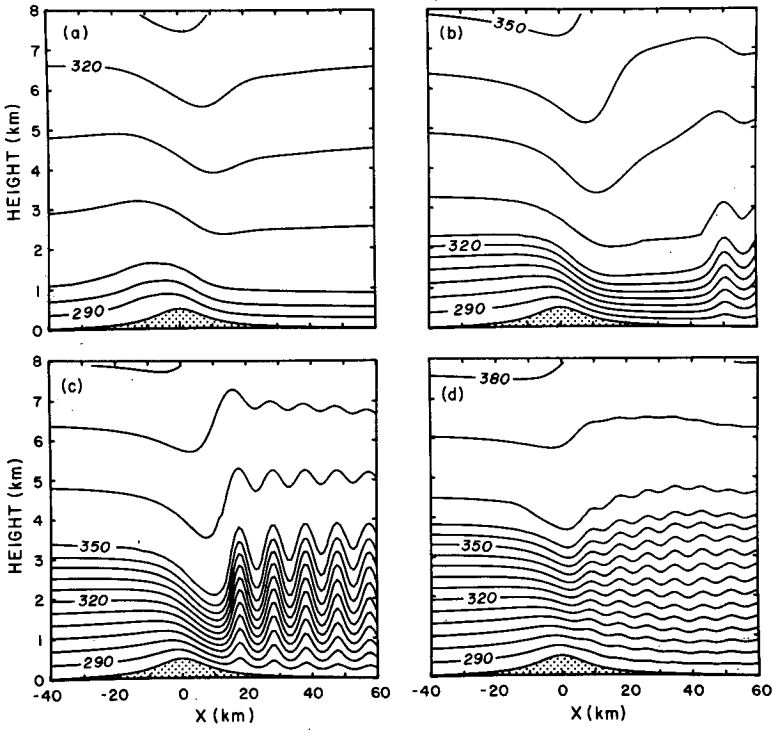


FIG. 5. Isentropes for the airflow in a two-layer atmosphere, at $Ut/a = 25$, when the mountain height is fixed at 500 m, and the interface is at (a) 1000 m, (b) 2500 m, (c) 3500 m and (d) 4000 m.

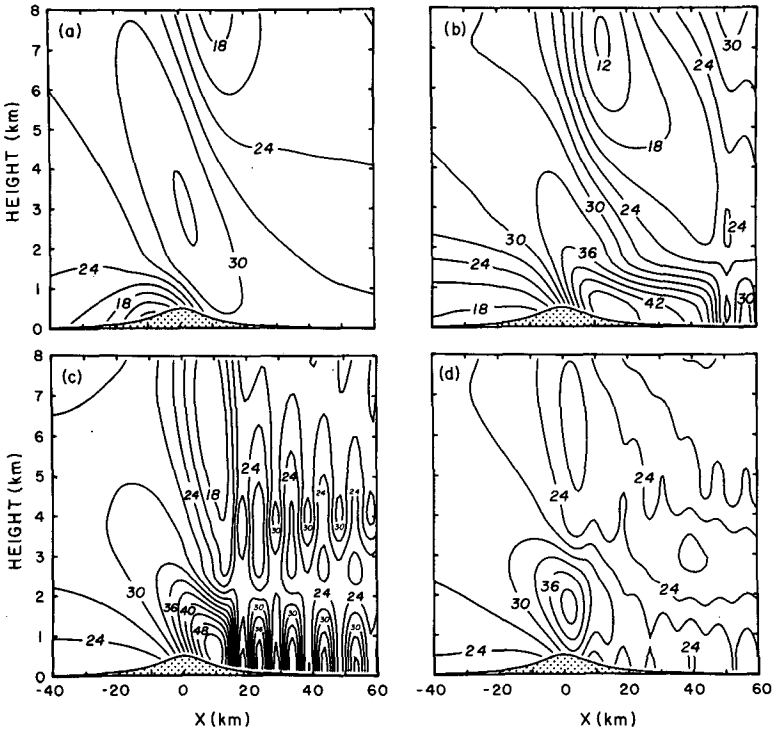


FIG. 6. As in Fig. 5, except that the plotted field is horizontal windspeed.

layer; $\pi = 3.1416$; and the mean cross-mountain windspeed is assumed to be constant with height. In the case under examination, only the $n = 1$ mode is subcritical with respect to the mean flow. We may define a Froude number with respect to the $n = 1$ mode as follows:

$$\mathrm{Fr}_1 = \frac{u}{c} = u(g'H)^{-1/2} \tag{8}$$

where

$$g' = \frac{4}{\pi^2} g \frac{\Delta\theta}{\theta_0}\left(1 - \frac{N_U^2}{N_L^2}\right). \tag{9}$$

In the preceding, $\Delta\theta$ is the potential temperature difference across the lower layer and $\theta_0$ is the mean potential temperature in the layer.

The Froude number, $\mathrm{Fr}_1$, was evaluated at the top of the mountain for each of the cases shown in Fig. 3; the results appear in Table 2. The behavior of $\mathrm{Fr}_1$ is analogous to that of the conventional Froude number in shallow water theory; the transition from subcritical to supercritical flow is associated with a sharp increase in the lee side winds (compare Table 2 with Fig. 4). However, it is difficult to attach much physical significance to this result because the nonhydrostatic effects essential for the production of trapped waves and the definition of $\mathrm{Fr}_1$ are not required for the production of the jumplike flow (see Fig. 2). Therefore, let us consider an alternate way of connecting hydraulic theory with the behavior of an infinitely deep, continuously stratified fluid with a single interface across which the stratification is discontinuous.

In conventional shallow water theory, the relationship between the slope of the free surface of a liquid flowing over an obstacle and the slope of the bottom topography may be written as

$$\frac{\partial z_s}{\partial x} = \left[1 - g\frac{(\delta_I + H - z_s)}{u^2}\right]\frac{\partial \delta_I}{\partial x} \tag{10}$$

(Long, 1954) where $z_s$ is the height of the topography, $\delta_I$ is the displacement of the free surface about its upstream height $H$, and $u$ is the horizontal speed of the fluid. This equation is derived from the steady state continuity and momentum equations. One may apply the "Boussinesq" continuity equation to the stratified case, and integrate between the ground and the layer interface to obtain an equation identical to the steady shallow water continuity equation

TABLE 2. Froude number at the crest as function of mountain height.

| Height of mountain (m) | $\mathrm{Fr}_1$ at mountain crest |
|---|---|
| 200 | 0.74 |
| 300 | 0.90 |
| 500 | 1.19 |
| 800 | 1.27 |

$$\frac{\partial}{\partial x}[\bar{u}(\delta_I + H - z_s)] = 0, \tag{11}$$

except that the horizontal windspeed becomes the layer-averaged windspeed in the stratified case. If one could also manipulate the $x$-momentum equation to obtain a form equivalent to the steady, shallow-water, momentum equation

$$\frac{u\partial u}{\partial x} + g\frac{\partial \delta_I}{\partial x} = 0, \tag{12}$$

it would be possible to produce an equation analogous to (10) for the relationship between the slope of the topography and the displacement of the layer interface in an infinitely deep stratified fluid. However, it is impossible to produce a suitable analog to the shallow water momentum equation (12) because there is no simple relationship between the pressure and the displacement of the layer interface (or any other material surface) in an unbounded stratified fluid.

The pressure perturbations in a shallow homogeneous fluid may be determined by integrating the hydrostatic equation between the height of the free surface and its undisturbed initial level. Let us perform a similar operation in a stratified fluid by integrating the hydrostatic equation between the perturbed and unperturbed locations of the interface. Suppose that the motion is isentropic and that $\delta(x, z)$ is the displacement of the isentrope, passing through the point $(x, z)$, above its initial height in the undisturbed flow. The difference between the potential temperature in the disturbed flow at the point $(x_0, z_0)$ and the potential temperature of the undisturbed environment may be approximated as

$$\Delta\theta(x_0, z_0) = \theta_0 - \left[\theta_0 + \delta(x_0, z_0)\frac{d\bar{\theta}}{dz}\right], \tag{13}$$

where $\theta_0$ is the isentrope in the disturbed flow passing through the point $(x_0, z_0)$. The buoyancy perturbation associated with this temperature difference is

$$g\frac{\Delta\theta}{\theta_{00}} = -N^2\delta \tag{14}$$

where $\theta_{00}$ is the mean temperature in the layer and the Boussinesq approximation has been invoked. Now suppose that after being displaced a distance $z^*$, the parcel encounters a level across which the mean stability in the undisturbed environment is discontinuous. In this case the difference in potential temperature becomes

$$\Delta\theta = \begin{cases} \theta_0 - \left[\theta_0 + z^*\left.\dfrac{d\bar{\theta}}{dz}\right|_L + (\delta - z^*)\left.\dfrac{d\bar{\theta}}{dz}\right|_U\right], & 0 < z^* < \delta \\ \theta_0 - \left[\theta_0 + z^*\left.\dfrac{d\bar{\theta}}{dz}\right|_U + (\delta - z^*)\left.\dfrac{d\bar{\theta}}{dz}\right|_L\right], & \delta < z^* < 0. \end{cases} \tag{15}$$

Here the notation $|_U$ ($|_L$) indicates that the quantity is to be evaluated in the upper (lower) layer. The geometry of the situation is shown in Fig. 7. The associated buoyancy perturbations are

$$g\frac{\Delta\theta}{\theta_{00}} = \begin{cases} z^*(N_U^2 - N_L^2) - \delta N_U^2, & 0 < z^* < \delta \\ z^*(N_L^2 - N_U^2) - \delta N_L^2, & \delta < z^* < 0. \end{cases} \tag{16}$$

In this equation, the second term represents the perturbations which would be produced if the fluid parcels never crossed the position of the undisturbed interface. The first term gives the correction required to account for cross-interface displacement.

The hydrostatic equation for the pressure perturbations may be written, subject to the Boussinesq approximation, as

$$\frac{\partial P}{\partial z} = g\frac{\Delta\theta}{\theta_{00}} \tag{17}$$

where $P = c_p\theta_{00}\pi$.

As a first-order approximation, $\delta = \delta_I$ and $z^* = \delta_I - z$, where $\delta_I$ is the displacement of the interface about its undisturbed position. Then the integral of the perturbation pressure between the interface and its undisturbed height, $P^*$, becomes

$$P^* = \begin{cases} \displaystyle\int_{\delta_I}^{0} z(N_L^2 - N_U^2) - \delta_I N_L^2 dz, & \delta_I > 0 \\ \displaystyle\int_{0}^{\delta_I} z(N_U^2 - N_L^2) - \delta_I N_U^2 dz, & \delta_I < 0 \end{cases} \tag{18}$$

or

$$P^* = \mathrm{sgn}(\delta_I)\frac{\delta_I^2}{2}(N_L^2 + N_U^2). \tag{19}$$

Equation (19) clearly is not a correct expression for the total perturbation pressure below the interface. However, it can be interpreted as that contribution to the total pressure produced by the displacement of the interface in a manner analogous to the displacement of the free surface in a homogeneous fluid. If we temporarily assume that the pressure perturbations are

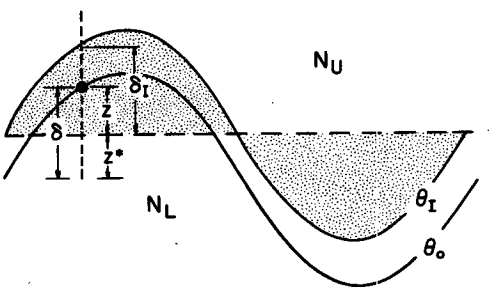


FIG. 7. Geometry of the disturbed interface. The interface coincides with the $\theta_I$ contour. Its undisturbed position lies along the dashed line.

dominated by the contribution from interface displacement, we obtain an $x$-momentum equation, similar to that in the shallow-water system, which can be combined with the integrated continuity equation to yield:

$$\frac{\partial z_s}{\partial x} = \left[1 - \frac{\text{sgn}(\delta_I)\delta_I(N_L^2 + N_U^2)(\delta_I + H - z_s)}{\bar{u}^2}\right]\frac{\partial \delta_I}{\partial x} \quad (20)$$

where $\bar{u}$ is the average horizontal windspeed in the lower layer. Equation (20) is clearly analogous to the conventional shallow water result (10), but its validity is contingent upon the total perturbation pressure being dominated by $P^*$. We will examine the numerical simulations to determine those regions where the pressure gradient is dominated by the contribution from the displacement of the interface and, in those regions, (20) must hold.

The total horizontal pressure gradient at a height just above the top of the mountain and the pressure gradient due to the displacement of the interface (i.e., the $x$ derivative of Eq. 19) are plotted in Fig. 8 for the four cases shown in Fig. 3. The pressure gradients have been normalized by $\rho NUh/a$. As the height of the mountain increases, the region of negative pressure gradient (which acts to accelerate the wind down the lee slope) extends progressively further toward the base of the mountain. In addition, as the flow becomes more nonlinear, the relative contribution from the displacement of the interface to the total pressure gradient increases along the lee side of the mountain and becomes dominant approximately halfway down the slope (Figs. 8c, d). Therefore, in the more nonlinear cases, a large portion of the lee-slope flow must be approximately governed by the hydraulic analog (20). In the same region where the pressure gradient is dominated by the contribution from the displacement of the interface, the Froude number,

$$\text{Fr}_2 = \bar{u}[\text{sgn}(\delta_I)(N_U^2 + N_L^2)\delta_I(\delta_I + H - z_s)]^{-1/2}, \quad (21)$$

is greater than 1, suggesting that the disturbance is basically a supercritical flow. Upstream of the mountain crest, the interface is not greatly disturbed, and the flow resembles a vertically propagating internal wave.

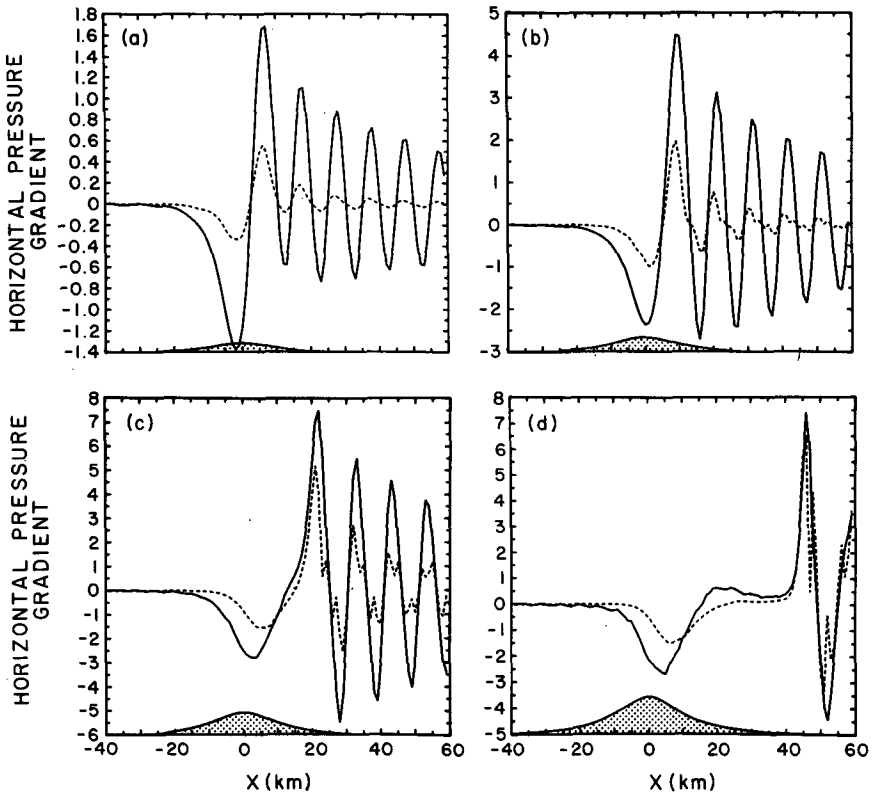


FIG. 8. Total horizontal pressure gradient, (solid) and horizontal pressure gradient associated with the displacement of the interface (dashed), as a function of horizontal distance across the mountain, for the cases shown in Fig. 3. The pressure gradient has been normalized by $\rho NUh/a$. The mountain contour is included at the bottom of the figure as a reference. Note that the difference between the two pressure gradients at any particular point is given by the *vertical* separation between the curves.

The phenomena shown in Figs. 3, 4 and 8 may be summarized as follows. When the height of the mountain is small, it forces a disturbance which is essentially a vertically propagating wave accompanied by weak lee waves. As the wave amplitude increases, the displacement of the interface also increases, and the pressure gradient associated with that displacement begins to dominate the total pressure gradient along the lee slope. As the pressure gradient induced by the displaced interface becomes dominant, the flow becomes constrained by (20). If the Froude number (21) in this region is greater than 1, a supercritical flow develops which is similar to that found in classical hydraulic jumps.

## 4. Discussion

The preceding diagnosis demonstrates that there is more than just a visual similarity between hydraulic jumps and the solutions shown in Figs. 3 and 5. The source of this similarity may be explained as follows. Consider first the flow of water over a rock. The water will always be in one of two basic states: subcritical or supercritical flow. In either case, at steady-state there is a three way balance between nonlinear advection, the pressure gradient due to changes in the thickness of the fluid, and the component of the gravitional acceleration parallel to the lower boundary. The ratio of the magnitudes of the first two terms in this balance is equal to the Froude number squared $\{\mathrm{Fr} = u[g(\delta_I + H - z_s)]^{-1/2}\}$. In supercritical flow, $\mathrm{Fr} > 1$, nonlinear advection dominates the pressure gradient term and the resulting acceleration is in the same sense as the gravitional force. Consequently, as a fluid parcel ascends the obstacle it slows, converting kinetic energy (KE) to potential energy (PE); after passing the crest, it reaccelerates as PE is converted back to KE (Fig. 9a). However in subcritical flow, $\mathrm{Fr} < 1$, the pressure gradient term dominates advection and balance is achieved when the resulting acceleration is directed opposite to the gravitional force. Then, as shown in Fig. 9b, a fluid parcel ascending the obstacle accelerates as the free surface drops and PE is converted to KE; after passing the crest it decelerates as KE is converted back to PE.

If there is a sufficient acceleration in the standing gravity wave, i.e., a sufficient increase in velocity and decrease in thickness as the fluid ascends toward the crest, a transition from subcritical to supercritical flow occurs at the top of the obstacle. This is illustrated in Fig. 9c. Since the flow along the lee slope is supercritical, the fluid continues to accelerate as it falls down the mountain; it eventually recovers to the ambient downstream conditions in a turbulent hydraulic jump. Very high velocities are produced along the lee slope because PE is converted to KE during the entire time that a fluid parcel is traversing the mountain. The deceleration of the fluid which would be produced in a leeside gravity wave is interrupted when the flow becomes supercritical. In a steady supercritical flow, it is impossible

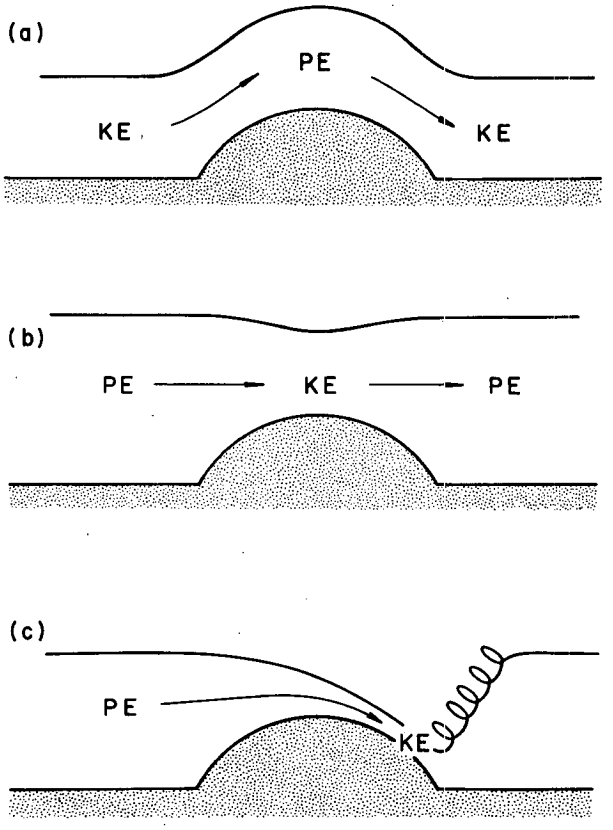


FIG. 9. Behavior of water flowing over an obstacle: (a) everywhere-supercritical flow, (b) everywhere-subcritical flow, (c) hydraulic jump.

to develop a horizontal pressure gradient through changes in the fluid's thickness that will counterbalance nonlinear advection without violating continuity. A more complete discussion of hydraulic theory may be found in Long (1954).

Roughly speaking, the same mechanism is active in the two-layer cases just examined, except that the role played by surface gravity waves in the liquid is played by vertically propagating (internal) gravity waves in the continuously stratified atmosphere. When a standing vertically propagating gravity wave is present over a mountain, the minimum surface winds occur approximately halfway up the windward slope. The winds increase downstream from that point, recovering to the speed of the ambient flow near the crest and reaching their maximum approximately halfway down the lee slope. Thus, like surface waves, vertically propagating internal waves allow air parcels to increase their PE as they ascend to the ridgeline, without experiencing any net deceleration.

If the wave amplitude is sufficiently large, the interface becomes important on the lee side of the crest (where the displacements in a small amplitude vertically propagating wave would produce a pressure gradient decelerating the low-level winds before they reach the bottom of the mountain). The perturbation pres-

sure associated with the displacement of the interface (19) may be written as

$$P^* = \mathrm{sgn}(\delta_I)\left[N_L^2\delta_I^2 - \frac{\delta_I^2}{2}(N_L^2 - N_U^2)\right], \quad (22)$$

which implies that a decrease in stability in the upper layer reduces the strength of the pressure perturbation associated with a given interface displacement, relative to that produced in an atmosphere with uniform stability. When the waves are sufficiently nonlinear, the reduction in the ability to produce pressure perturbations by displacing the interface leads to a supercritical flow. (As in conventional hydraulic theory, the terminology "supercritical flow" characterizes a situation where the perturbations in the fluid cannot produce a horizontal pressure gradient capable of balancing nonlinear advection.) When the flow is supercritical, kinetic energy is no longer returned to potential energy in a leeside gravity wave, and the air continues to accelerate as it falls down the mountain.

There are factors other than the interface displacement that affect the pressure perturbations in vertically propagating internal waves; these have been neglected in the preceding argument. However, as shown in Fig. 8, in those circumstances where strong leeside winds occur, the pressure perturbations associated with displacements of the interface make a dominant contribution to the total pressure gradient along the lee slope, suggesting that the neglect of the other factors is permissible.

Although several studies have shown that linear theory seriously underestimates the amplitude of trapped lee waves (Smith, 1976; Peltier and Clark, 1979; Durran and Klemp, 1982), the rapid breakdown of linear theory, as applied to vertically propagating waves, has not been previously documented. This author is not aware of any simulations that have been conducted with the specific intention of testing the effects of nonlinearity on linear gravity wave reflection concepts. Klemp and Lilly (1978) do describe three simulations in which the effects of nonlinearity are investigated in a two-layer atmosphere with a 6°C km$^{-1}$ lapse rate in the lower layer and an isothermal upper layer. They found little difference between the normalized drag in a linear case and the drag in a second case where Nh/U had a maximum value of 1.04. These simulations have been repeated with the numerical model used in the current investigation, and the results appear to confirm those obtained by Klemp and Lilly, suggesting that this is a situation, like case 3 (Table 1), in which linear theory produces a good approximation to the actual nonlinear response. At any rate, this is the only case they discuss, and it is not ideally configured to test the linear partial reflection mechanism because the stability is not constant in the lower layer (it varies between 0.115 and 0.0130 s$^{-1}$), and the depth of the lowest layer is not optimally tuned to produce the strongest amplification or damping from those reflections which do occur.

Smith (1977) has examined the second-order correction to the linear solution for waves in a two-layer atmosphere and found that the second-order contribution should tend to reinforce any amplification or damping predicted by first-order linear theory. This would appear to be in conflict with our numerical results, except that he only considered forcing by sinusoidal topography at a single wavenumber. It is likely that the difference in the results is due to the absence of horizontal periodicity and the presence of a wide spectrum of horizontal wavenumbers in the numerical solution.

## 5. The Boulder windstorm of 11 January 1972

It should be emphasized that the static stabilities and windspeeds used in the preceding experiments are representative values for the earth's atmosphere. A typical value for the static stability averaged across the troposphere is 0.01 s$^{-1}$; a stability of 0.02 s$^{-1}$ is characteristic of an isothermal layer. The factor of 2.5, by which the stability changes across the interface in the later experiments, could frequently be observed at the top or bottom of an inversion layer. However, the soundings used in these experiments do differ from those typically observed in the actual atmosphere in that there is no vertical wind shear and the stable layer in the lower troposphere is unusually deep. Therefore, let us examine the contribution that the transition from subcritical to supercritical flow makes in the development of an actual windstorm.

Figure 10 shows the isentrope field from a simulation of the severe windstorm which occurred in Boulder, Colorado, on 11 January 1972. In this simulation, the numerical grid and atmospheric structure have been configured to match those used in earlier studies by Peltier and Clark (1979) and Durran and Klemp (1983). The computational domain contains 180 grid points in the horizontal and 44 grid levels in the vertical; the grid intervals are $\Delta x = 1000$ m, $\Delta z = 341$ m. The large and small time steps are 5 and 2.5 s. The mountain is centered at grid point 70 and is specified by (6), with $a = 10$ km and $h = 2$ km. The upstream windspeed and temperature profiles are those determined by Peltier and Clark from the 1200 GMT 11 January Grand Junction sounding. Only a windowed portion of the full domain is shown in Fig. 10.

Two additional simulations are shown in Figs. 11 and 12. They are identical to the standard case shown in Fig. 10, except that the upstream atmospheric profile has been modified in an attempt to isolate the factors which are most important for the development of the storm. In the case shown in Fig. 11, the stability in the elevated inversion has been reduced to match the average tropospheric stability. In the case shown in Fig. 12, the stratospheric stabilities and windspeeds have been replaced with the stability and windspeed observed at the top of the troposphere. The time-evolution

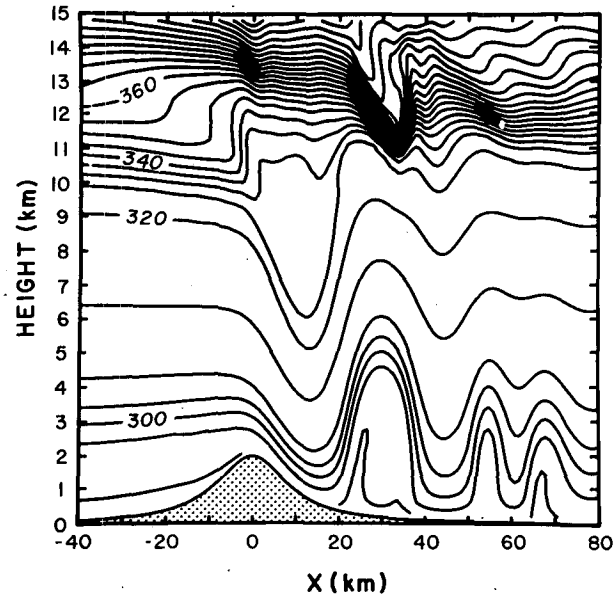


FIG. 10. Isentropes from a simulation of the 11 January 1972 Boulder windstorm using the upstream conditions observed at Grand Junction, at a model time of 12000 s.

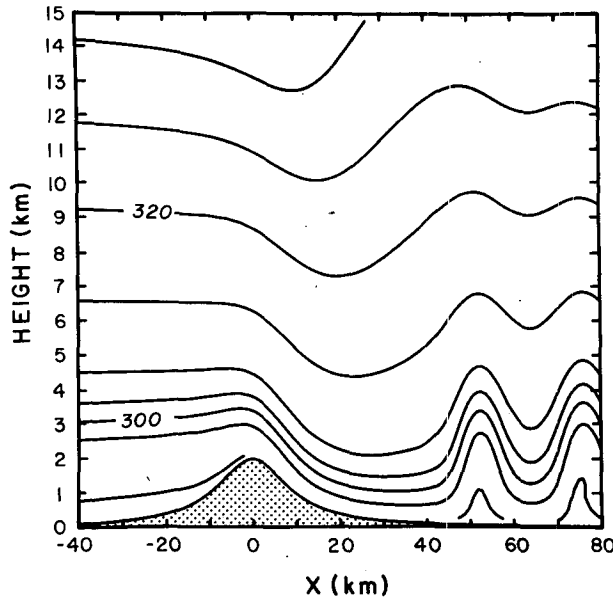


FIG. 12. As in Fig. 10, except that the upstream sounding has been modified to remove the stratosphere.

of the surface pressure drags for all three cases is compared in Fig. 13.

When there is no elevated inversion (Fig. 11), the tropospheric waves are feeble, and the pressure drag is small. However, as the wave enters the stratosphere, where $N/U$ increases, it steepens just to overtuning (minimum horizontal winds less than 1 m $s^{-1}$ but not less than 0). The steepened region remains essentially steady for the last 5000 s of the simulation; during this time the disturbance shows no tendency toward amplification.

When the stratosphere is eliminated (Fig. 12), a relatively strong response is rapidly produced as a region of supercritical flow (defined in this case with respect to the pressure perturbation produced by the vertical displacement of the entire inversion layer) develops along the lee slope. The drag stops increasing when the shooting flow reaches the base of the mountain. Prior to a time of 8000 s, the pressure drag is actually stronger

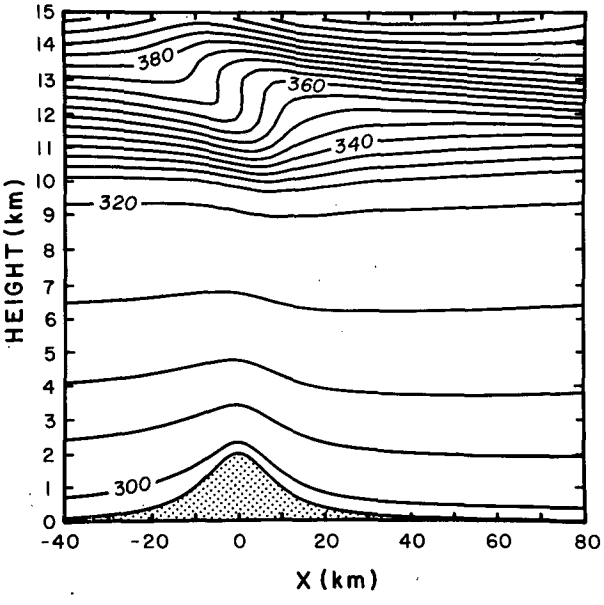


FIG. 11. As in Fig. 10, except that the upstream sounding has been modified to remove the elevated inversion.

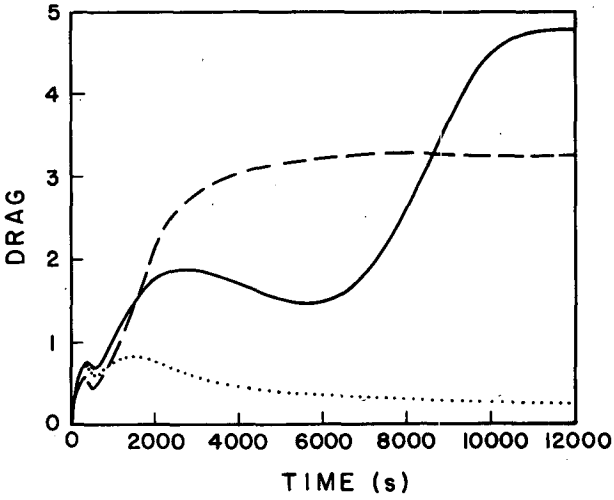


FIG. 13. Pressure drag, normalized by $\pi\rho NUh^2/4$ (where $\rho$, $N$ and $U$ are evaluated at the surface) as a function of time for the cases in Fig. 10 (solid), Fig. 11 (dotted), and Fig. 12 (dashed).

than that which develops in the standard 11 January simulation. The two examples in Figs. 11 and 12 seem to support the hypothesis that an important nonlinear amplification mechanism responsible for the development of downslope winds is the transition from a gravity wave structure upstream to a supercritical flow along the lee slope. The absence of the elevated inversion prevents the development of the supercritical flow and eliminates the windstorm. On the other hand, when the inversion is retained but the change in atmospheric structure at the tropopause is eliminated (thereby preventing breaking and eliminating an important reflecting interface for vertically propagating waves), a significant windstorm still develops.

The strongest response occurs when the atmospheric structure matches that observed on 11 January. As shown in Fig. 13, there are two separate periods during which the surface wave drag increases rapidly. During the first period, the displacement of the elevated inversion produces a region of shooting flow which propagates down to the base of the lee slope. This is the same amplification mechanism which is active in the case shown in Fig. 12. However, another process is responsible for the amplification which occurs after 5500 s, and, as emphasized by Peltier and Clark (1979), it appears to be associated with wave breaking.

## 6. Wave breaking

Since the amplification mechanism associated with wave breaking does not become active until the waves have already become quite strong, our first goal has been to explore the factors which produce large amplitude, nonbreaking waves. It has been suggested that these waves often develop when there is a transition from subcritical to supercritical flow over the crest of the mountain, analogous to that described by hydraulic theory. Recently, there has been an increased awareness that the flow which develops when breaking waves are present resembles a hydraulic jump (Clark and Peltier, 1984; Pierrehumbert and Wyman, 1985; Smith 1985; Klemp and Durran, 1986). At present there is still some question whether this similarity is superficial or substantive.

The only extensive numerical simulations of breaking waves have been conducted by Clark and Peltier (1977, 1984), Peltier and Clark (1979, 1983) and Clark and Farley (1984), who first discovered the importance of breaking as a nonlinear amplification mechanism. Clark and Peltier have proposed that the amplification is produced when energy is reflected from the overturned layer and trapped in the cavity between the ground and the reversed flow. They have generally deemphasized the similarity between breaking waves and hydraulic jumps. In the following, we will present numerical simulations which more extensively document the similarities between the flow beneath a breaking wave and a supercritical flow. In these cases, the atmosphere has a uniform mean wind of 10 m $s^{-1}$ and stability N of 0.01 $s^{-1}$. The mountain is given by (6) with a half-width of 10 km; $\Delta x$ and $\Delta z$ are 1 km and 250 m respectively; the large and small time steps are 10 and 2 s. There are 120 grid points in the horizontal and 48 points in the vertical.

The wave drag and surface windspeed maximum (again normalized by their values calculated from the linear solution) are plotted as a function of mountain height in Fig. 14. If the mean density did not decrease with altitude, overturning should occur whenever the height of the mountain exceeds 850 m (Miles and Huppert, 1969). In these simulations, the decrease in density allows the flow to overturn at the second steepening level when the mountain height is only 750 m. The breaking region influences the flow below it, so that the streamlines at the first steepening level also eventually overturn. Since this entire process happens rather slowly, the points associated with the 750 m mountain are plotted twice in Fig. 14. One point reflects the pseudosteady values attained before the wave breaks at the first steepening level; the second point shows the values attained after breaking.

Figure 14 may be compared with Fig. 4; note that in both instances there are distinct low drag and high drag regimes. In the two-layer atmosphere the transition to the high drag regime is associated with the development of supercritical flow along the lee slope (i.e., the breakdown of the leeside gravity wave). In a single-layer atmosphere, the transition to the high drag regime is associated with the development of breaking waves (Clark and Peltier, 1977). Thus, breaking acts in a manner analogous to the transition to supercritical flow. As discussed earlier, there is no limit on the maximum phase speed of linear waves in an infinitely deep, continuously stratified fluid so the flow cannot be supercritical with respect to these waves. However, the well-mixed reversed flow in the overturned region provides a different effective upper boundary condition which places new constraints on the modal structure of all gravity waves in the layer between the overturned region and the ground. It may be possible for the flow

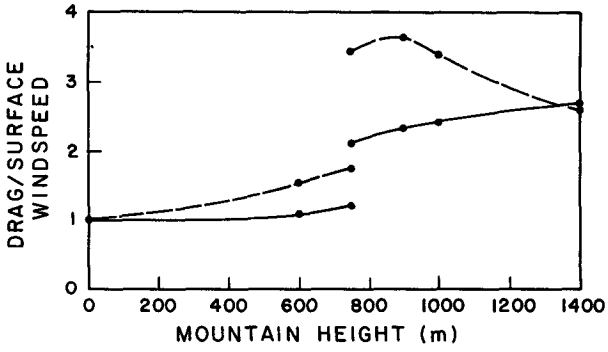


FIG. 14. As in Fig. 4, except the data were obtained from simulations in which the mean windspeed and stability are constant.

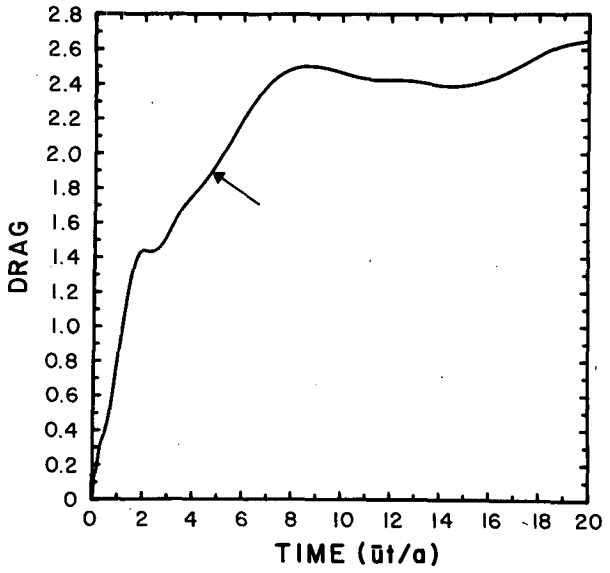


FIG. 15. Pressure drag, normalized by $\pi\rho NUh^2/4$, as a function of nondimensional time ($Ut/a$), for a case with uniform windspeed and stability in which $Nh/U = 1.4$.

to be supercritical with respect to these modes. The most important influence of the new effective upper-boundary condition may be due either to the presence of reversed flow (Clark and Peltier, 1984) or neutral stability (Smith, 1985).

The time-dependent development of the pressure drag across the mountain is shown in Fig. 15 for the case in which $Nh/U = 1.4$. The drag increases rapidly for the first two units of nondimensional time ($Ut/a$), while the model is initialized by increasing the gravitational constant and the mean windspeed from zero to their appropriate final values. Then there is a six-unit period during which the drag increases almost linearly; the time when overturning first occurs, which is marked on the figure, is near the middle of this period. The drag remains approximately constant for the last 12 units. The evolution of the flow is also illustrated by the isentropes displayed in Fig. 16 and the horizontal velocity fields shown in Fig. 17. Note that the wave drag stops increasing once the shooting flow, which develops under the breaking region, arrives at the base of the mountain. Note also that once the nose of the shooting flow passes a particular point on the lee slope, the windspeed at that point stops increasing. This behavior is consistent with the idea that the air parcels are essentially falling down the mountain under the influence of gravity.

The vertical flux of horizontal momentum, $\overline{pu'w'}$, integrated across the total width of the domain and normalized by the flux associated with the linear so-

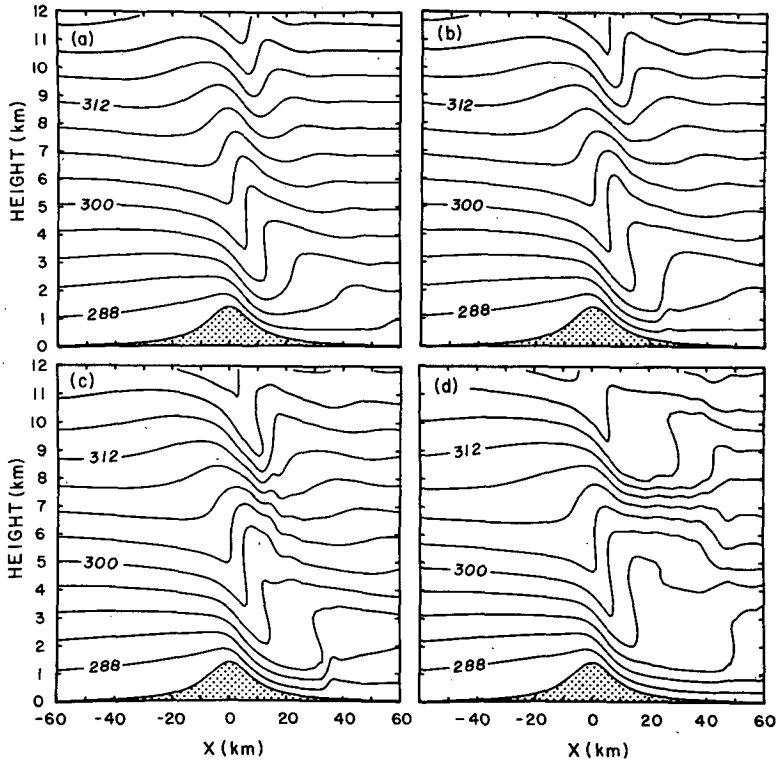


FIG. 16. Isentropes for the airflow in an atmosphere with constant mean windspeed and stability in which $Nh/U = 1.4$, at nondimensional times of (a) 6, (b) 8, (c) 10, (d) 18.

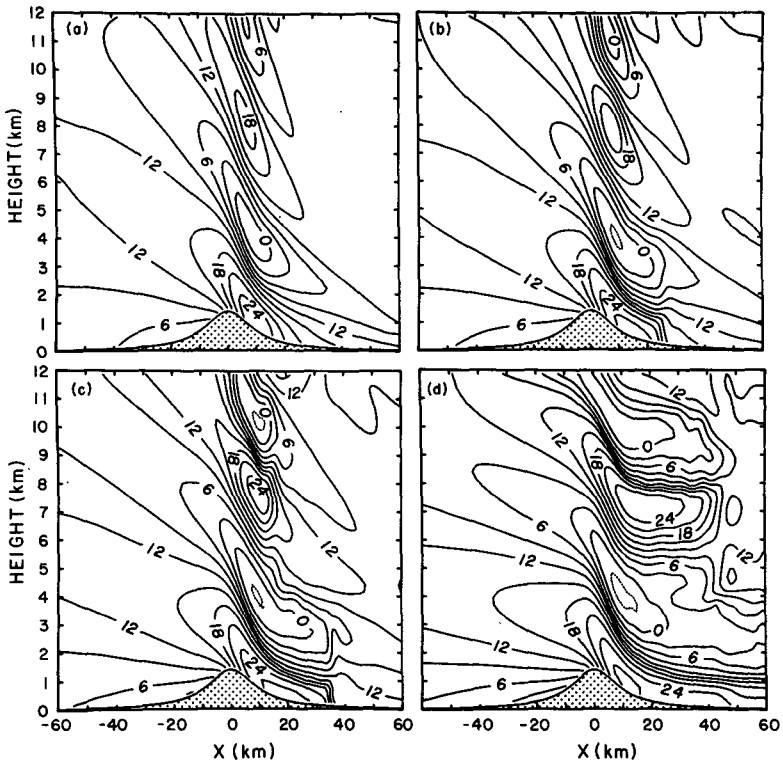


FIG. 17. As in Fig. 16, except that the plotted field is horizontal windspeed.

lution, is plotted against height in Fig. 18a for this same case ($Nh/U = 1.4$). The vertical profile of the normalized momentum flux for the two-layer case in Fig. 3c (no breaking) is presented in Fig. 18b as a reference. In both simulations, the momentum flux profiles have reached a nearly steady state, and there is a sharp gradient in the flux near the ground, implying that a large fraction of the energy in the disturbance is trapped in the lower atmosphere. However, in both cases the decrease in the vertical energy flux with height does not produce a continual increase in the wave amplitude over the mountain; instead, it appears to be balanced by downstream transport. In the multilayer case, where the waves do not break, this is accomplished by both the downstream propagation of the laminar "jump" at the end of the shooting flow, and by trapped waves,

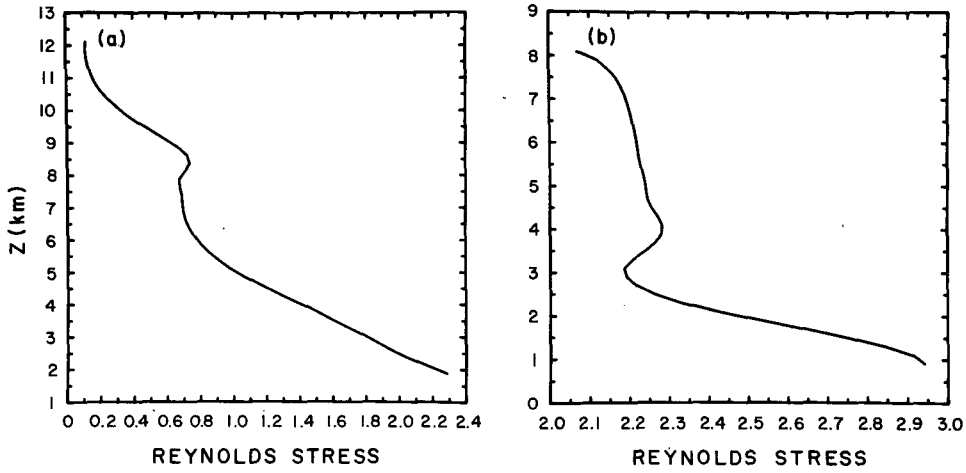


FIG. 18. Vertical flux of horizontal momentum, normalized by $\pi\rho NUh^2/4$, as a function of height for (a) the case in Figs. 16 and 17 at $Ut/a = 10$ and (b) the case in Fig. 3c at $Ut/a = 25$.

whose group velocity is directed downstream. In a single-layer atmosphere, in which breaking waves are present, the most important transport mechanism is the downstream propagation of the shooting flow and the turbulent jump which accompanies it.

These simulations seem to be entirely consistent with those obtained by Peltier and Clark (1979; see particularly Fig. 6–9), although they have been continued to larger nondimensional times. They do not imply that the basic critical layer reflection mechanism proposed by Peltier and Clark is in error, but they do suggest that an alternative framework, based on hydraulic theory, may also be used to explain the amplification associated with wave breaking.

## 7. Conclusions

We have examined the manner in which finite amplitude solutions differ from those predicted by linear theory when the mean atmospheric windspeed is constant and the stability has a two-layer structure. In some circumstances, linear theory was found to underpredict the pressure drag by more than 500%; in other situations linear theory overpredicted the drag by a factor of 2; in yet another case there was essentially no difference between the linear and finite amplitude results. When the stability has a multilayer structure, nonlinear effects become significant at rather small values of $Nh/U$. In one case, in which the maximum value of $Nh/U$ was 0.3, the drag in the linear and nonlinear cases differed by a factor of 3. In contrast, there would be only a negligible difference between the linear and nonlinear solutions in a single-layer atmosphere in which $Nh/U = 0.3$.

The largest differences between the linear and nonlinear solutions and the cases with the strongest downslope winds occurred when the flow underwent a transition from a standing gravity wave structure upstream of the mountain to what appears to be a supercritical flow along the lee slope. In these cases the static stability in the lower layer exceeded that in the upper layer. Numerical experiments in which either the depth of the lower layer was varied while the mountain height was held fixed, or the depth of the lower layer was fixed and the mountain height varied, produced results which are qualitatively identical to the flow of water over a rock. The similarity with hydraulic theory was quantified by comparing the total horizontal pressure gradient in the lower layer with the pressure gradient produced by displacements of the interface. In those cases where the flow exhibited a large-amplitude response, the pressure perturbations associated with the interface displacement dominated the other contributions to the total pressure perturbation along the lee slope, and therefore the flow was constrained to be supercritical. It was suggested that the presence of lower stability in the upper layer promotes the development of supercritical flow by reducing the ability of the fluid to develop a lee-side pressure gradient capable of decelerating the low-level wind.

The importance of the hydraulic amplification mechanism was demonstrated in numerical simulations of the 11 January 1972 Boulder windstorm. When the storm was simulated using the observed data, an initial amplification of the surface wind and pressure drag occurred as a low-level inversion was displaced downward along the lee slope, producing a supercritical flow. At a later point in the simulation, the gravity waves associated with this disturbance break in the upper troposphere, producing further amplification of the disturbance. If this inversion is removed from the upstream sounding, the initial amplification phase is eliminated, and no windstorm develops (although a small region of wave breaking does appear in the lower stratosphere). If the low-level inversion is retained but the stratosphere is replaced by an infinite troposphere, breaking is eliminated, but a moderately strong windstorm is still produced by the transition to supercritical flow. The idea that elevated inversions play a crucial role in the generation of downslope winds is consistent with the observational studies of Colson (1954) and Brinkmann (1974), who found that they are almost always present in the lower troposphere on days when there are strong mountain waves and downslope winds. Further observational support is provided by Bower and Durran (1986), who documented a situation in which there was no elevated inversion and downslope winds did not occur, even though all other factors appeared very favorable for windstorm development.

Although the primary emphasis in this paper has been on the amplification of inviscid nonlinear waves, wave breaking has been examined in an atmosphere in which the mean wind and stability were constant. It was suggested that the current which develops beneath the breaking region closely resembles a supercritical flow. In that case, a single fundamental nonlinear amplification mechanism, the transition from a gravity wave structure upstream of the mountain crest to a supercritical flow along the lee side, can be used to explain the development of the high fluid velocities which occur in the lee of an obstacle in a variety of similar geophysical phenomena. These phenomena include the flow of water over a rock in a hydraulic jump and the development of downslope winds, with or without wave breaking, in the atmosphere.

*Acknowledgments.* The author greatly benefited from conversations with Joe Klemp, Rich Rotunno, Doug Lilly, Ron Smith and Chris Bretherton. Jan Paegle provided suggestions which improved the manuscript. Part of this work was conducted while the author was visiting NCAR's Mesoscale Research Section. This research was supported by NSF Grant ATM-8320695. Computational facilities were provided by NCAR's Scientific Computing Division.

## APPENDIX

### Subgrid Scale Mixing Terms

The subgrid scale mixing terms used in the calculation of the velocity fields are

$$D_u = \frac{\partial}{\partial x}(K_M A) + \frac{\partial}{\partial z}(K_M B),$$

$$D_w = \frac{\partial}{\partial x}(K_M B) - \frac{\partial}{\partial z}(K_M A), \tag{A1}$$

where

$$A = \left(\frac{\partial u}{\partial x} - \frac{\partial w}{\partial z}\right), \quad B = \left(\frac{\partial u}{\partial z} + \frac{\partial w}{\partial x}\right), \tag{A2}$$

$$K_M = k^2 \Delta x \Delta z (A^2 + B^2)^{1/2} \left[\max\left(1 - \frac{K_H}{K_M}\mathrm{Ri}, 0\right)\right]^{1/2}, \tag{A3}$$

$$\mathrm{Ri} = \frac{N^2}{A^2 + B^2}. \tag{A4}$$

The subgrid scale mixing terms used in the thermodynamic equation are

$$D_\theta = \frac{\partial}{\partial x}\left(K_H \frac{\partial \theta}{\partial x}\right) + \frac{\partial}{\partial z}\left(K_H \frac{\partial \theta}{\partial z}\right), \tag{A5}$$

where $K_H/K_M = 3$.

## REFERENCES


Blumen, W., and C. S. Hartsough, 1985: Reflection of hydrostatic gravity waves in a stratified shear flow: Part II. Application to downslope surface windstorms. *J. Atmos. Sci.*, **42**, 2319–2331.

Bower, J. B., and D. R. Durran, 1986: A study of wind profiler data collected upstream during windstorms in Boulder, Colorado. *Mon. Wea. Rev.*, **114**, 1491–1500.

Brinkmann, W. A. R., 1974: Strong downslope winds at Boulder, Colorado. *Mon. Wea. Rev.*, **102**, 592–602.

Clark, T. L., and W. R. Peltier, 1977: On the evolution and stability of finite-amplitude mountain waves. *J. Atmos. Sci.*, **34**, 1715–1730.

——, and ——, 1984: Critical level reflection and the resonant growth of nonlinear mountain waves. *J. Atmos. Sci.*, **41**, 3122–3134.

——, and R. D. Farley, 1984: Severe downslope windstorm calculations in two and three spatial dimensions using anelastic interactive grid nesting: A possible mechanism for gustiness. *J. Atmos. Sci.*, **41**, 329–350.

Colson, DeVer, 1954: Meteorological problems in forecasting mountain waves. *Bull. Amer. Meteor. Soc.*, **35**, 363–371.

Durran, D. R., and J. B. Klemp, 1982: The effects of moisture on trapped mountain lee waves. *J. Atmos. Sci.*, **39**, 2490–2506.

——, and ——, 1983: A compressible model for the simulation of moist mountain waves. *Mon. Wea. Rev.*, **111**, 2341–2361.

Houghton, D. D., and A. Kasahara, 1968: Nonlinear shallow fluid flow over an isolated ridge. *Commun. Pure Appl. Math.*, **21**, 1–23.

Klemp, J. B., and D. K. Lilly, 1975: The dynamics of wave induced downslope winds. *J. Atmos. Sci.*, **32**, 320–339.

——, and ——, 1978: Numerical simulation of hydrostatic mountain waves. *J. Atmos. Sci.*, **35**, 78–107.

——, and D. R. Durran, 1983: An upper boundary condition permitting internal gravity wave reflection in numerical mesoscale models. *Mon. Wea. Rev.*, **111**, 430–444.

——, and ——, 1986: Numerical modelling of bora winds. *Meteor. Atmos. Phys.*, (in press).

Lilly, D. K., and J. B. Klemp, 1979: The effects of terrain shape on nonlinear hydrostatic mountain waves. *J. Fluid. Mech.*, **95**, 241–261.

——, and ——, 1980: Comments on the evolution and stability of finite-amplitude mountain waves. Part II: Surface wave drag and severe downslope windstorms. *J. Atmos. Sci.*, **37**, 2119–2121.

Long, R. R., 1953: Some aspects of the flow of stratified fluids I, A theoretical investigation. *Tellus*, **5**, 42–58.

——, 1954: Some aspects of the flow of stratified fluids II, Experiments with a two fluid system. *Tellus*, **6**, 97–115.

Miles, J. W., and H. E. Huppert, 1969: Lee waves in a stratified flow. Part 4. Perturbation approximations. *J. Fluid Mech.*, **35**, 497–525.

Orlanski, I., 1976: A simple boundary condition for unbounded hyperbolic flows. *J. Comput. Phys.*, **21**, 251–269.

Peltier, W. R., and T. L. Clark, 1979: The evolution and stability of finite-amplitude mountain waves. Part II: Surface wave drag and severe downslope winds. *J. Atmos. Sci.*, **36**, 1498–1529.

——, and ——, 1980: Reply. *J. Atmos. Sci.*, **37**, 2122–2125.

——, and ——, 1983: Nonlinear mountain waves in two and three spatial dimensions. *Quart. J. Roy. Meteor. Soc.*, **109**, 527–548.

Pierrehumbert, R. T., and B. Wyman, 1985: Upstream effects of mesoscale mountains. *J. Atmos. Sci.*, **42**, 977–1003.

Smith, R. B., 1976: The generation of lee waves by the Blue Ridge. *J. Atmos. Sci.*, **33**, 507–519.

——, 1977: The steepening of hydrostatic mountain waves. *J. Atmos. Sci.*, **34**, 1634–1654.

——, 1985: On severe downslope winds. *J. Atmos. Sci.*, **42**, 2597–2603.